Sintering and characterization of HA and TCP bioceramics with control of their strength and phase purity

A. TAMPIERI, G. CELOTTI, F. SZONTAGH* and E. LANDI
IRTEC-CNR, via Granarolo 64, 48018 Faenza, Italy
** Department of Silicate Chemistry and Technology, University of Veszprem, Hungary*

HA and β-TCP-based ceramics were prepared using commercial powders. Powder characteristics were defined and the processing parameters studied, aimed at the production of samples with improved microstructural and mechanical properties. The behaviour of HA powder subjected to various thermal treatments was investigated in order to control the formation of secondary phases (α- and β-TCP) during sintering. The optimal thermal treatment required to prepare pure β-TCP powder from the precursors (HA and DCP) was determined and the sintering method required to prepare fully dense β-TCP completely free from α-form, was identified. Translucent hot-pressed β-TCP ceramics with potential applications in aesthetic restorative prostheses were prepared and characterized. The interval of existence of $\bar{\alpha}$-TCP and α-TCP as secondary products was also defined. Crystallographic analysis was carried out on the imperfectly known low-temperature $\bar{\alpha}$-TCP phase, and a proper monoclinic unit cell determined.

1. Introduction

Calcium phosphates are major constituents of bone, and hold great promise as biomaterials for bone implantation since they have the ability to bond to bone. The major phase found in bone is HA ($Ca_5(PO_4)_3OH$), however, very often defective HA occurs with a Ca/P ratio which deviates from 1.67 [1, 2]. Among these secondary phases, we focus attention on α-TCP ($Ca_3(PO_4)_2$).

Porous HA implants have been widely used in various fields (orthopaedics, maxillofacial, etc.) and have demonstrated bone in-growth into the open pores on the surface of the implant. Similar studies [3] have shown that dense HA and β-TCP implants become surrounded by mature fibrous tissue with a variable amount of new bone formation. Because of their bioactivity calcium phosphate implants are expected to create good contact with bone and to reduce the problems of rejection. As a result of its peculiar characteristics, HA and β-TCP could be considered promising materials for biomedical applications.

Up to now calcium phosphate structural implants have been characterized by poor mechanical properties: the tendency to develop cracks [4, 5] requires optimization of the material microstructure and control of the compositional evolution to improve the material strength.

At temperatures $T \geqslant 1200\,^{\circ}C$, HA becomes unstable and tends to eliminate OH groups and to form decomposition products [6]. Among them, α-TCP and β-TCP often form during sintering of the material. In particular the molecular volume increase occurring in the transformation β → α-TCP seems to be the most deleterious phenomenon for the mechanical properties [7].

As regards β-TCP, it presents the same problem caused by thermal treatment as described for HA, and in addition the difficulty of obtaining pure compound starting from the precursors HA and $CaHPO_4$ [8].

The present study aims to prepare dense and pure bulk HA and β-TCP materials suitable for clinical applications and characterized by improved mechanical properties, and discusses the formation of α-TCP and related phases at different stages of thermal treatment.

2. Experimental procedures

Spray-dried HA powder and a precursor powder for TCP, consisting of a stoichiometric molar mixture 1:1 of HA and DCP ($CaHPO_4$), were supplied by Jesse–Shirley. Both powders were characterized by X-ray diffraction (XRD), using a Rigaku diffractometer operating with graphite monochromatized CuK_α radiation. From the peak intensities and the scattering powers, using α-Al_2O_3 as a reference standard, volume fractions of the various phases detected were evaluated. Powders morphology was examined by scanning electron microscopy (SEM) (Leica Cambridge).

Mean particle size was determined by Sedigraph (Micromeritics): an ultrasound treatment to disperse the particles in ethanol was applied.

0957–4530

Thermoanalytical investigations (TG, DTA) were performed in the temperature range 20–1550 °C with a heating rate of 10 °C/min using a Netzsch instrument capable of an accuracy of 2×10^{-5} g.

The evolution of phases, with particular attention to α-TCP, was followed directly by a special Rigaku high temperature attachment (maximum 1500 °C) on the XRD instrument that allows study of reversible transformations.

The shrinkage of cold isostatically pressed (100 MPa) bars was recorded as a function of temperature by Netzsch dilatometer.

Sintering tests were carried out in the temperature range 1220–1300 °C for HA and 1220–1260 °C for β-TCP; in both cases the heating programme was 50 °C/h up to 600 °C, then 200 °C/h up to the final temperature, maintained for 1 h, followed by subsequent free cooling in the furnace. With TCP, hot-pressing tests were performed in a graphite die at 1150 °C for 1 h with 30 MPa applied load. Density was measured by Archimedes method and relative values were calculated assuming, as a reference, 3.13 g/cm^3 for HA and 3.07 g/cm^3 for β-TCP.

Flexural strength was determined on polished bars suitably shaped ($30 \times 3 \times 3$ mm) by a four-point bending device (Instron) with outer span 20 mm, inner span 10 mm and crosshead speed 0.5 mm/min.

3. Results and discussion

3.1. Hydroxyapatite

HA powder was shown to be pure under XRD examination. Powder morphology is reported in Fig. 1, showing nearly spherical agglomerates (18–22 μm in diameter) of globular grains with average diameter 0.5 μm. The average particle size determined by Sedigraph was 0.5 μm because the ultrasound treatment causes disaggregation of the agglomerates into primary particles, and particle size distribution results are necessarily very large.

In order to improve powder compaction, 1.5 wt % of organic binder (PVA) was added.

Thermoanalytical investigations performed on powders with suitable additives (Fig. 2) showed elimination of the organic phase at $200 \leqslant T \leqslant 420$ °C, through a corresponding weight loss in the TG curve. A further weight loss of about 1.8% was detected at temperatures higher than 800 °C, attributed to the elimination of hydroxyl groups. The weight loss detected at temperatures higher than 1400 °C is attributed to the elimination of CO_2 from CO_3^{2-} substituting PO_4^{3-}. Infrared analysis of the powder shows the presence of carbonate ions, indicated by bands at 880, 1420 and 1460 cm^{-1}. The weight loss ($\approx 0.5\%$) could correspond to the presence of ≈ 0.1 mole of CO_3^{2-} in each $Ca_{10}(PO_4)_6O$ mole. Finally the DTA peak at around 1450 °C corresponds to HA decomposition and subsequent melting of some decomposition products [6].

Usually the sintering temperature for HA powders is chosen in the range 1150–1350 °C: depending on starting powder features, the lower temperature is defined by the excess in residual porosity at grain boundaries, and the higher one by the advancement in the degradation process.

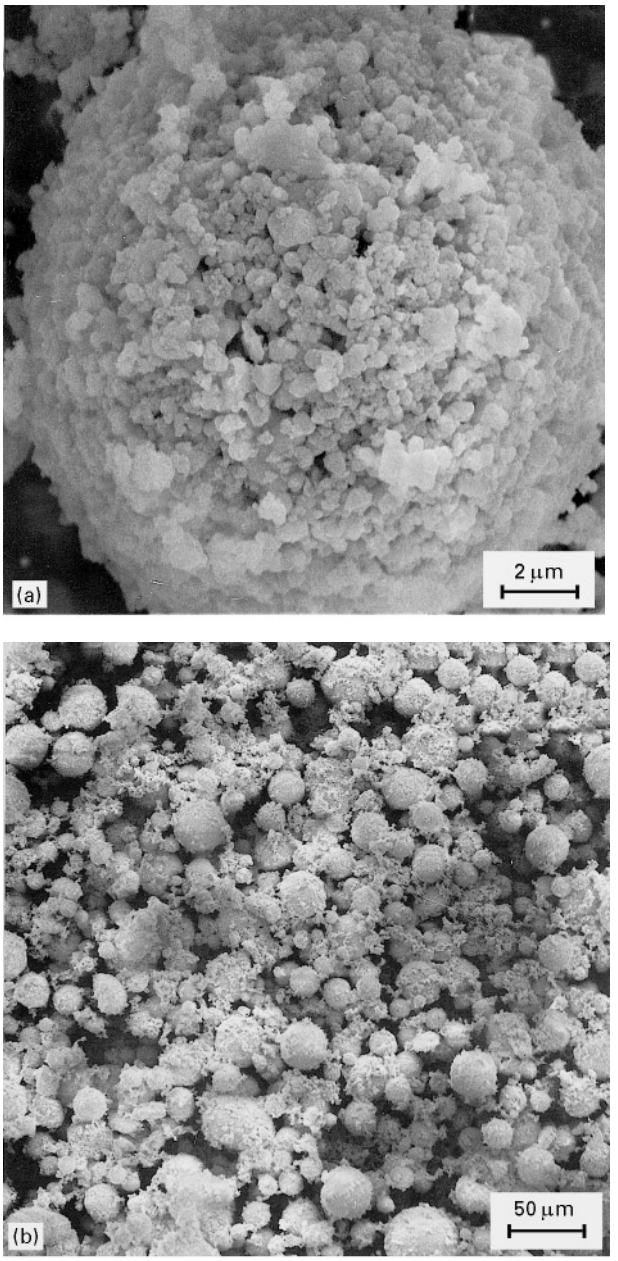

Figure 1 SEM micrographs showing: (a) HA agglomerate; (b) morphology of HA powder.

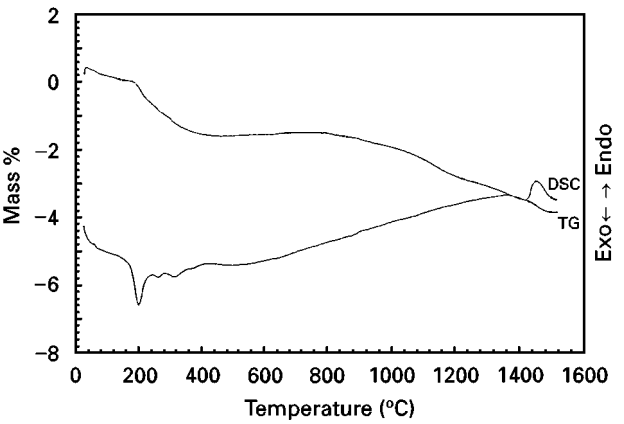

Figure 2 DTA and TG analysis for the HA powder (the total weight loss was 4.12%).

Shrinkage has been analysed as a function of temperature and is shown in Fig. 3. In Fig. 3a two steps

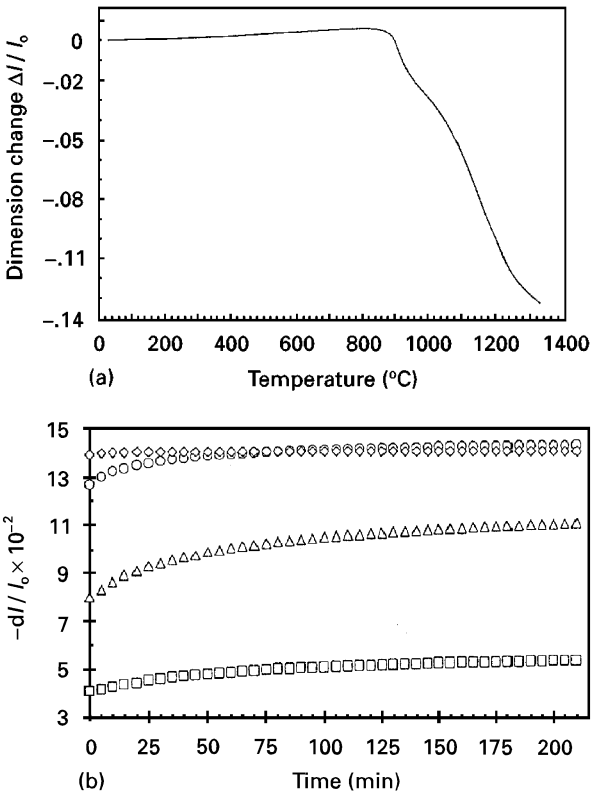

Figure 3 (a) Dilatometric curve indicating the shrinkage of debonded HA powder as a function of temperature; (b) densification versus time for HA material: □ 1000 °C; △ 1100 °C; ○ 1200 °C; ◇ 1300 °C.

can be identified; the first one of about 2% corresponds to the effect of water elimination resulting in cell volume contraction. The second one, starting at 950 °C, represents the sintering period, from which the best densification range can be determined (1100–1300 °C). In Fig. 3b the densification behaviour under isothermal conditions at different temperatures is reported, limiting the optimal sintering temperature to the interval 1200–1300 °C in which complete densification is attained.

Owing to the determinant role played by secondary phases if formed during sintering, phase composition evolution was followed directly by an XRD high temperature attachment: it was found that, starting at 1200 °C, a small amount of β-TCP (1–3%) begins to appear, remaining almost constant up to 1250 °C. When the temperature exceeds 1250 °C, equivalent quantities of α-TCP (implying the already mentioned volume increase) are detected. Staying at 1300 °C for 100 min, no time-dependent compositional difference was observed: ≈ 3% β-TCP and ≈ 3% α-TCP.

Phase composition does not change during cooling, unless this process is very rapid compared to a classical furnace (around 500 °C/h), where amorphization of secondary phases can be expected.

The isostatically pressed bars were sintered at temperatures in the range 1220–1280 °C: the characteristics of green bodies and sintered materials are reported in Table I.

Relative density values range from about 92 up to 98%. An increase in sintering temperature beyond 1250 °C causes an increase in secondary phase content as determined by XRD. At 1250 °C the sintered samples comprise almost pure HA, and relative density values are greater than 97%. On the other hand, increase of the temperature to 1260 °C causes the formation of about 3% α-TCP; a further increase to 1280 °C results in the appearance of about 3% α-TCP, 4% β-TCP, and sometimes, traces of $Ca_4(PO_4)_2O$ (TeCP) and CaO.

Morphological evolution of the fracture surface of sintered samples is shown in Fig. 4a, b, c, in which gradual reduction of intergranular porosity occurs in going from 1220 °C to 1280 °C, together with slight grain growth from ≈ 2 μm to ≈ 8 μm. A peculiar morphology can be observed starting at 1260 °C: the typical polyhedric grains begin to coalesce, forming large necks that at 1280 °C yield large tabular grains; at times an amorphous layer is observable. High values of flexural strength ($\sigma \approx 130$ MPa) [9] were measured in samples sintered at 1250 °C (Table I), while at lower and higher sintering temperatures reduced σ values were found. Two explanations can account for these results: (i) composition almost monophasic compared to the other temperatures, stimulating the formation of impurities, mainly α- and β-TCP, which are known to transform into each other with deleterious volume variations; (ii) homogeneous microstructure characterized by optimal grain size (4–5 μm): lower temperatures imply incomplete densification and diffuse porosity, higher temperatures led to rapid and excessive grain growth, leaving occasional sinks of ungrown grains (Fig. 5).

Both these aspects depress flexural strength; in the first case because of the lack of a tight link among the grains, in the second case because of the presence of inhomogeneities acting as critical defects.

Fig. 6a shows the fresh fracture surface of a high-flexural-strength HA sample. The study of fracture origin reveals that usually cracks are generated at specimen surface defects, therefore, as previously observed [9], remarkable improvement can be achieved by use of extremely well-polished samples. It is

TABLE I Characteristics of HA samples

Sample code	Relative green density (%)	Sintering temperature (°C)	Relative density (%)	Linear shrinkage (%)	Impurity phases (vol %)	σ (MPa)
H1	63.5	1220	93.0	13.0	–	50
H2	63.0	1250	97.5	14.5	–	130
H3	63.5	1260	98.0	13.5	α3	–
H4	63.0	1280	98.7	15.0	α2, β3	98
H5	62.5	1300	98.4	14.8	α3, β3	94

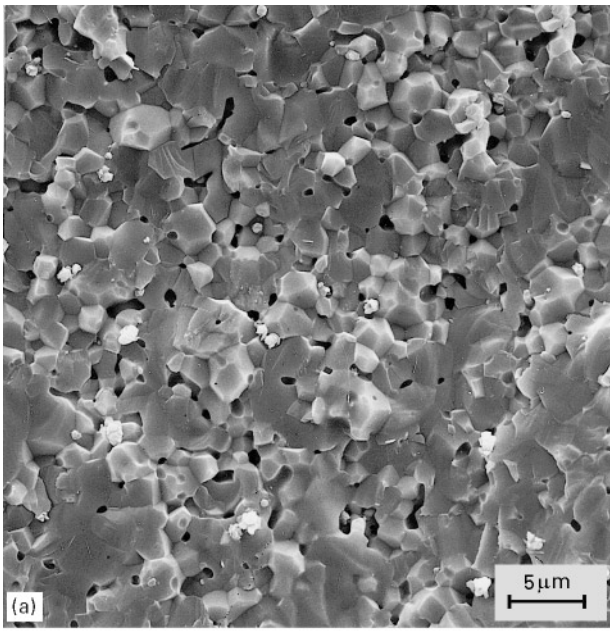

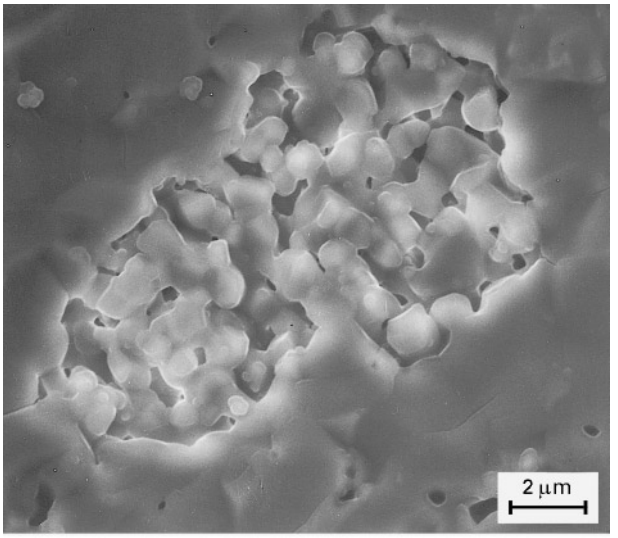

Figure 5 Detail of fracture surface of HA sample sintered at 1260 °C for 1 h.

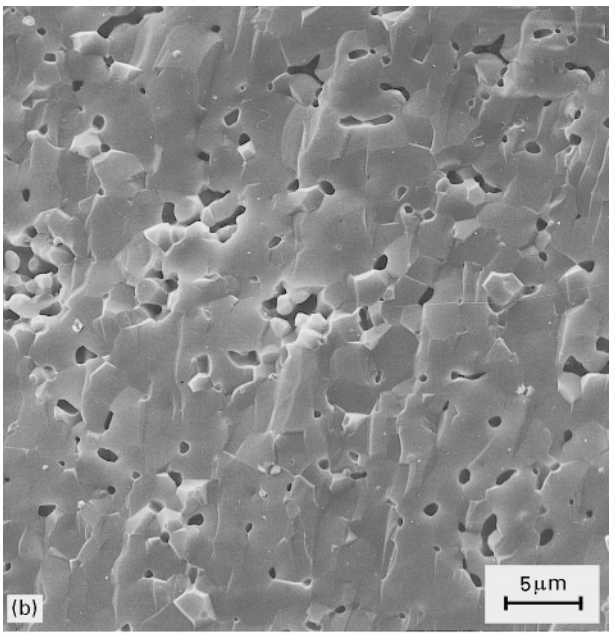

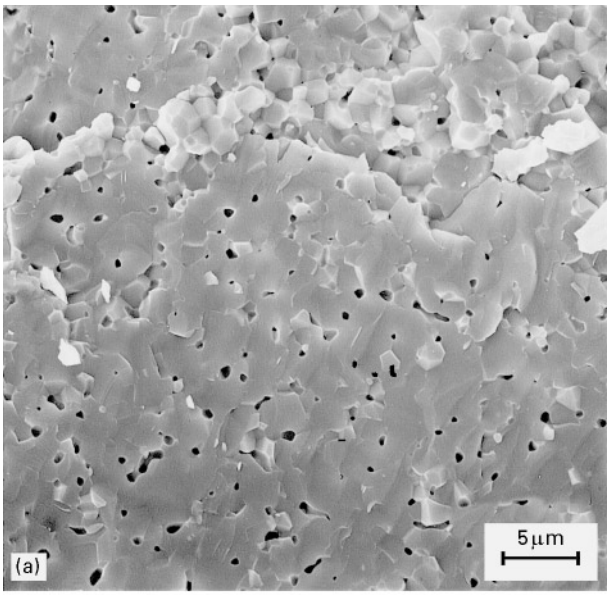

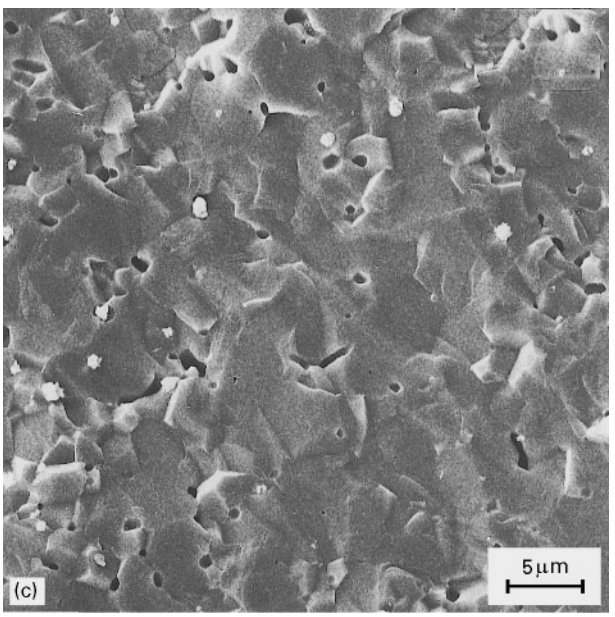

Figure 4 Morphology of fracture surfaces of HA sample: (a) sintered at 1200 °C for 1 h; (b) sintered at 1260 °C for 1 h; (c) sintered at 1300 °C for 1 h.

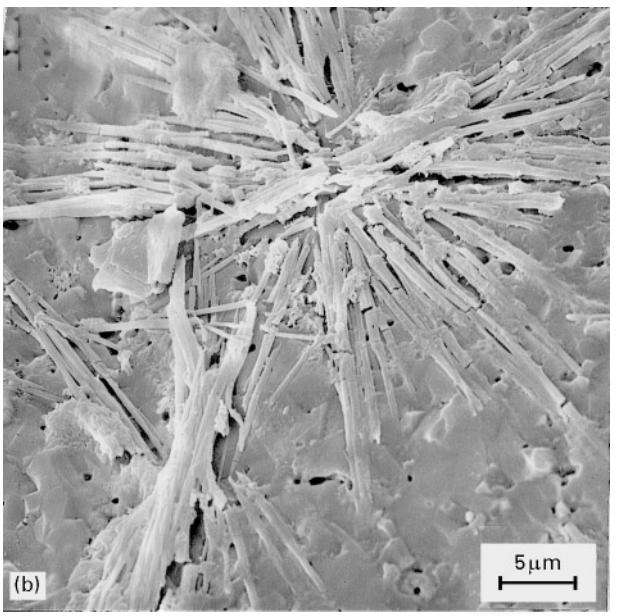

Figure 6 Morphology of fracture surface of HA sample sintered at 1250 °C for 1 h: (a) freshly exposed; (b) after 1 month of ageing in contact with atmospheric moisture.

worthwhile mentioning that such a surface, if left in contact with atmospheric moisture for long enough, forms degradation products (Fig. 6b). XRD analysis of the aged surface identified these needle-like structures as $CaHPO_4$, $CaHPO_4 \cdot 2H_2O$ and $Ca(OH)_2$.

The high σ-values, comparable only with samples prepared with powders produced by mechanochemical synthesis [10], can be attributed to the particular powder characteristics: good packing ability, thanks to the favourable grain size and distribution, involving high density in the green bodies and high surface reactivity leading to lower sintering temperature, which limits grain growth and weakens impurity phases formation.

3.2. Tri-calcium phosphate

The morphology of spray-dried precursor powder for TCP preparation is shown in Fig. 7, consisting of spherical agglomerates with average size 10–15 mm formed by primary irregular particles of size ≈ 0.2 μm.

TG-DTA analysis, reported in Fig. 8, shows the reactions between the precursors to form β-TCP. The TG curve reveals a total weight loss of about 4.8%: the first step, starting at about 50 °C and completed at 500 °C, is attributed to the elimination of organic binder ($\approx 3\%$) present in the commercial precursor. At ≈ 750 °C a second step, corresponding to a weight loss of $\approx 1.5\%$, indicates the elimination of H_2O as a consequence of the reaction between HA and DCP. The complete reaction should involve a weight loss of 2.8%, therefore in this case it is possible to deduce an incomplete reaction leaving HA and DCP among the reaction products.

It is interesting to note in the DTA curve the endothermic peak at ≈ 800 °C related to the reaction among precursors, followed by another peak at ≈ 1200 °C corresponding to the transformation $\beta \rightarrow \alpha$-TCP and two sharp peaks at $T = 1415°$ and 1450 °C. The first peak can be attributed to the melting (see ICDD card no. 9-345) of pyrophosphate ($Ca_2P_2O_7$, CPP), resulting from the condensation reaction of the residual $CaHPO_4$, and the latter to the decomposition of unreacted HA. From these results the synthesis temperature of 900 °C has been defined in order to prepare β-TCP as pure as possible, avoiding the formation of any significant amount of α-TCP.

Precursor powder, reacted at 900 °C for 1 h, resulted in 89% β-TCP and 11% of unreacted HA; no α-TCP was detected.

In the particular case of TCP, whose formation in the solid state occurs from a stoichiometric mixture of HA and DCP, it was found necessary to perform direct temperature observations using a XRD high temperature attachment. Attention was focused on three temperature ranges: $T \leqslant 750$ °C, 800 °C $\leqslant T \leqslant 960$ °C and $T \geqslant 1100$ °C, to control the formation of low-temperature α-TCP (usually called ᾱ-TCP) and high-temperature α-TCP, as well as the complete reaction between the precursors.

In the low-temperature range one can still observe the precursors (Table II) that begin to react, forming

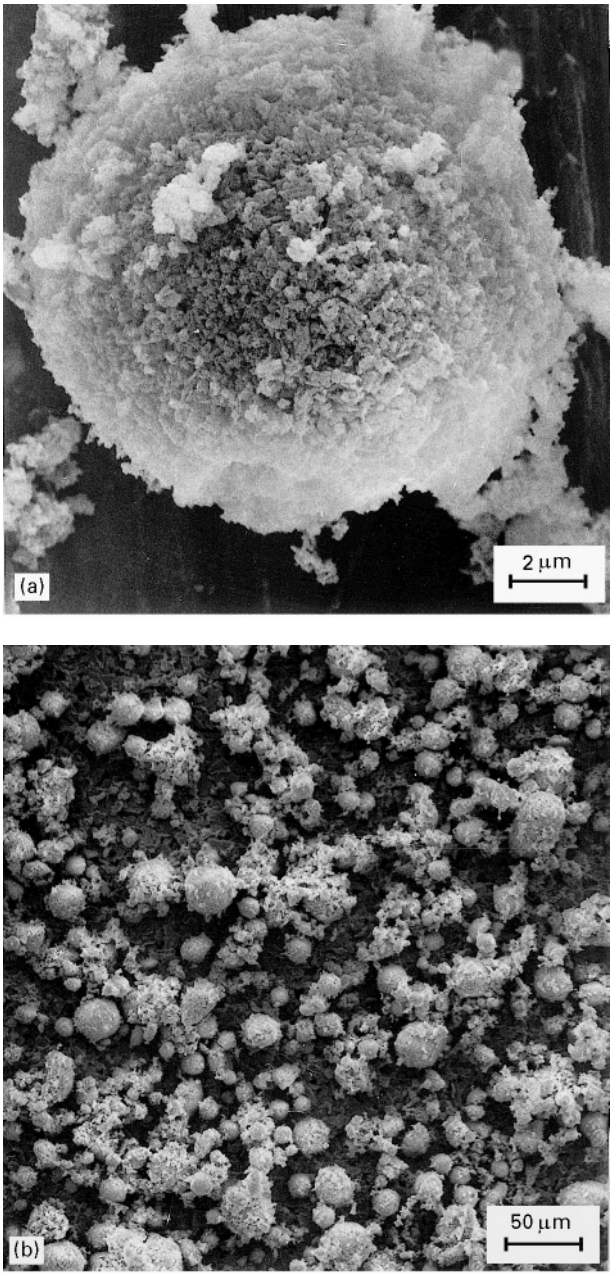

Figure 7 SEM micrographs showing: (a) TCP powder agglomerate; (b) morphology of TCP powder.

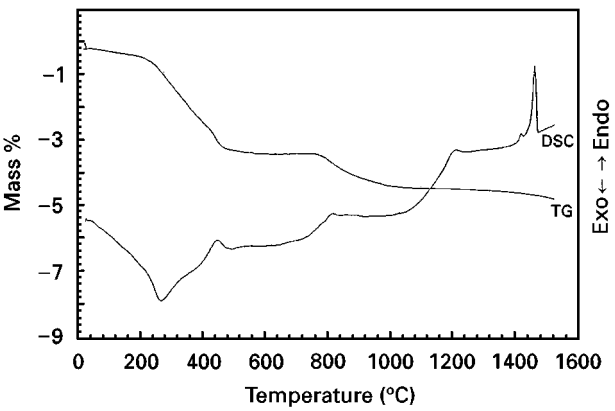

Figure 8 DTA and TG analysis of TCP powder (the total weight loss was 4.80%).

increasing amounts of ᾱ-TCP. Holding at 750 °C for about 30 min induces the temporary appearance of β-TCP. The total amount of TCP tends to decrease

TABLE II Percentage volume fractions of phases observed in TCP by XRD high-temperature attachment

Recording temperature (°C)	HA	DCP	$\bar{\alpha}$-TCP	β-TCP	α-TCP	Total TCP
25	77	23	–	–	–	–
650	75	19	6	–	–	6
700	73	14	13	–	–	13
750	76	9	15	–	–	15
750 (30 min)	71	5	13	11	–	24
25	72	9	11	8	–	19
25	77	23	–	–	–	–
800	66	7	–	27	–	27
830	48	–	–	52	–	52
860	36	–	–	64	–	64
900	30	–	–	70	–	70
930	22	–	–	72	6	78
960	16	–	–	74	10	84
800	20	–	–	72	8	80
600	20	–	–	75	5	80
400	20	–	–	77	3	80
25	24	–	–	74	2	76
25 (reacted)	8	–	–	92	–	92
1100	8	–	–	87	5	92
1200	10	–	–	81	9	90
1300	13	–	–	15	72	87
1200	15	–	–	20	65	85
1100	14	–	–	30	56	86
1000	16	–	–	31	53	84
900	17	–	–	34	49	83
25	17	–	–	33	50	83

TABLE III Characteristics of TCP samples

Sample code	Relative green density (%)	Sintering temperature (°C)	Relative density (%)	Linear shrinkage (%)	Phase composition (vol %)	σ (MPa)
T1	58.8	1220	91.0	13.6	α 62, β 29, HA9	75
T2	59.0	1250	91.6	–	α 62, β 28, HA10	–
T3	59.5	1260	92.2	14.0	α 64, β 26, HA10	100
HP	–	1150/30 MPa	100	–	β 89, HA11	120

during cooling to room temperature, in favour of the more stable HA phase. A parallel tendency for $\bar{\alpha}$-TCP to decrease in isothermal conditions, as well as during cooling, can be inferred.

In the intermediate temperature range, formation of the maximum amount of β-TCP is observed: at $T = 900\,^{\circ}C$ the β-TCP volume fraction is 70%, with no traces of α-TCP; the formation of α-TCP is detected starting at 930 °C; the highest concentration of TCP is found at 960 °C, consisting of 74% β-TCP and 10% α-TCP.

During cooling, while β-TCP remains nearly constant, α-TCP tends to disappear, making the total TCP concentration lower; a slight increase of unreacted HA can also be detected. It seems reasonable to suppose that the α-TCP, unstable in this temperature range, transforms to β-TCP which in turn partially converts to HA.

Using pellets made from reacted powder the high temperature range was investigated in order to observe the sintering phenomena. The gradual transformation of β-TCP into α-TCP up to 1200 °C becomes dramatic at 1300 °C; an increase of β-form at the expense of α is detected during cooling, accompanied by limited HA recrystallization. However, from all these measurements it is possible to show an always-incomplete formation of β-TCP and the unavoidable presence of a non-negligible amount of HA, and to determine the precise temperature interval of the existence of the two different phases: $\bar{\alpha}$- and α-TCP. A more complete explanation of the reaction path and the kinetics involved in β-TCP formation will be the subject of a forthcoming paper.

The characteristics of the green bodies and sintered materials are reported in Table III. The isostatically pressed bars were sintered at temperatures in the range 1220–1260 °C. The maximum relative density attained was $\approx 93\%$ and the morphology of samples sintered at 1260 °C is shown in Fig. 9. Mechanical properties improve with increasing sintering temperature ($\sigma \approx 80$ MPa at 1220 °C; $\sigma \approx 100$ MPa at 1260 °C).

To improve final density and to avoid the formation of α-TCP (whose formation, involving volume expan-

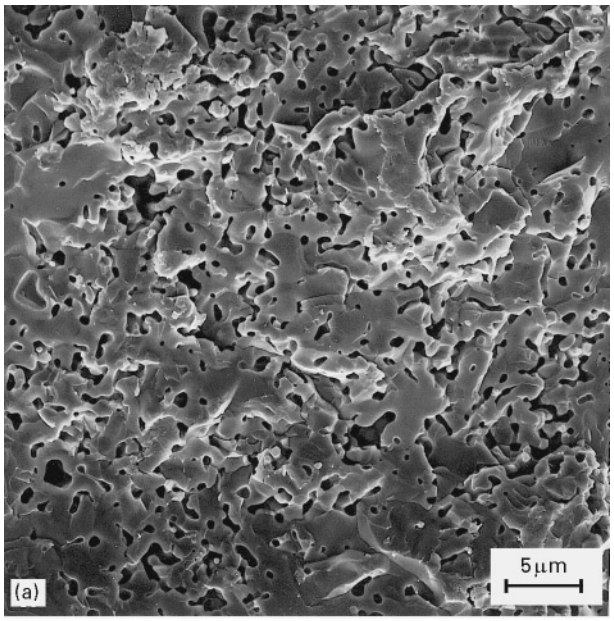

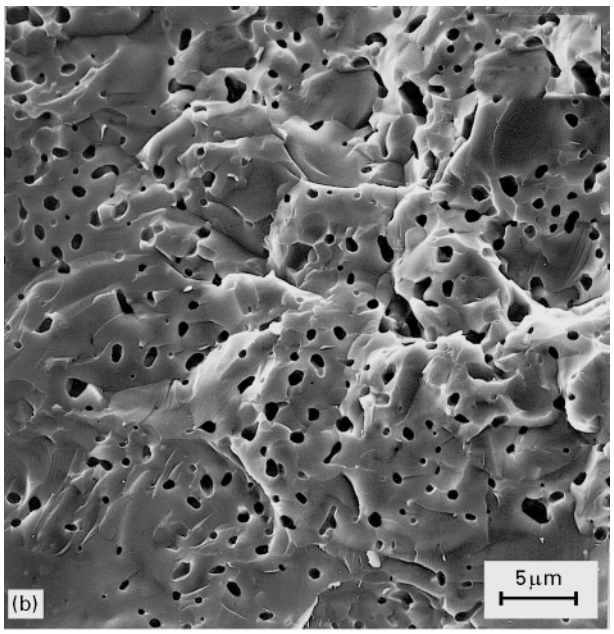

Figure 9 Morphology of fracture surfaces of TCP samples: (a) sintered at 1220 °C for 2 h; (b) sintered at 1260 °C for 2 h.

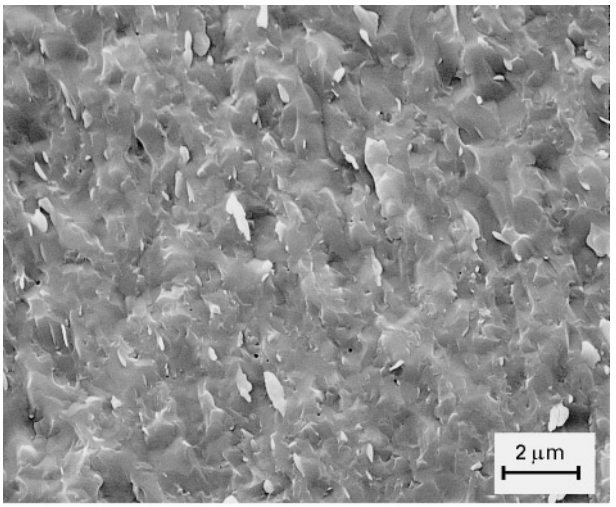

Figure 10 Morphology of fracture surface of TCP sample hot-pressed at 1150 °C, 30 MPa for 1 h.

sion, could be inhibited by pressure) the use of pressure sintering was considered. Hot pressed pellets reached full density, and XRD patterns reveal no α-TCP and ≈ 10% of HA left unreacted.

The morphology of hot pressed β-TCP is reported in Fig. 10, showing an average grain size ≈ 1–2 μm and tight grain packing, completely porosity free. Flexural strength results were improved ($\sigma \approx$ 120 MPa) by the above factors.

Owing to the incompleteness of data regarding low-temperature α-TCP (metastable α-TCP, sometimes called $\bar{\alpha}$ or α′-TCP) [11–13], usually found during thermal crystallization of amorphous calcium phosphate, a careful crystallographic investigation was performed on a sample containing a significant amount of this form to attempt individuation of the unit cell. The fundamental characteristics of this phase are: (i) practically undistinguishable from the well-known high-temperature phase (α-TCP); (ii) form, always in moderate concentrations, only between ≈ 600° and ≈ 800 °C; (iii) then vanish well before the appearance of α-TCP ($T > 900$ °C) [13–15].

The accuracy of this determination cannot be very high, due to the small amounts of interesting phase usually involved (in the range of ≈ 15 vol %) and the unavoidable temporary presence of two or three other phases. However, research focused on the small scattering angles region (in particular $2\theta \leqslant 10.5°$), where the main phases do not show appreciable diffraction effects, allowed (with low scanning speed and long counting times) detection of the many very weak peaks reported in Table IV. The reproducibility of the observed lines up to $2\theta = 35°$ was tested on at least six different patterns: the region of angles $2\theta > 35°$ can be considered, with the involved cells, as the scarcely significant "easy matching" zone.

The recorded data were generally found similar to the stanfieldite ($Ca_4(Mg, Fe)_5(PO_4)_6$) structure (ICDD card no. 20-223), existing also as $Ca_3Mg_3(PO_4)_4$ (ICDD card no. 11-234). Accounting for properly increased lattice parameters due to the actual stoichiometry $Ca_3(PO_4)_2$, tentative indexing was carried out on the basis of a monoclinic well with $a = 1.778$, $b = 1.033$, $c = 2.363$ nm, $\beta = 101°$, which results in a volume very close to α-TCP (suggesting $Z = 24$, $\rho = 2.90$ g/cm^3).

This indexing turned out to be completely successful, not only in justifying the new reflections, but in reproducing all the observed patterns (ICDD cards no. 9-348 and 29-359) of α-TCP also. This can be considered as a possible explanation of the distinction between XRD patterns of $\bar{\alpha}$-TCP and α-TCP: the former, even though characterized by a different cell, has its main reflections just overlapping those of the latter. Moreover, well-defined geometrical relationships exist between the two cells (Fig. 11): the unique axes b can be taken as coincident (with lengths almost in the ratio $b(\alpha):b(\bar{\alpha}) = 8:3$), while a and c axes are rotated so as to yield crystallographic plane superpositions $(2\,0\,0)_\alpha \equiv (3\,0\,1)_{\bar{\alpha}}$, $(0\,0\,4)_\alpha \equiv (1\,0\,7)_{\bar{\alpha}}$, $(10\,0\,0)_{\bar{\alpha}} \equiv (7\,0\,\bar{2})_\alpha$, $(0\,0\,10)_{\bar{\alpha}} \equiv (\bar{1}\,0\,6)_\alpha$.

TABLE IV Reflections observed in powder pattern of $\bar{\alpha}$-$Ca_3(PO_4)_2$ (angular range $5^\circ \leqslant 2\theta \leqslant 35^\circ$ with CuK_α radiation)

d (nm)	h k l	Intensity	Overlapping α-$Ca_3(PO_4)_2$ reflections d (nm)	h k l
1.54	$10\bar{1}$	vw		
1.29	101	vw		
1.16	002	vw	} 1.23	} 001
1.06	$10\bar{2}$	w		
1.03	010	vw		
.944	011	w		
.892	102, 110	vw		
.874	200, $20\bar{1}$	vw		
.858	$11\bar{1}$	w		
.773	003, 012, 201, $20\bar{2}$	w		
.762	$10\bar{3}$	vw		
.740	$11\bar{2}$	w	.731	031
.677	112	vw	.685	130
.666	103, 210, $21\bar{1}$	vw		
.642	202, $20\bar{3}$	w		
.620	013, 211	w	} .631	} $20\bar{1}$
.615	$11\bar{3}$, $21\bar{2}$	vw	.614	002
.592	$30\bar{1}$	vw		
.583	004, $10\bar{4}$, 300	w	.584	$13\bar{2}$
.562	113, $30\bar{2}$	vw		
.546	212, $21\bar{3}$	vw		
.515	020, $30\bar{3}$, $31\bar{1}$	w	.518	131
.507	014, 021, $11\bar{4}$, 310	vw		
.495	120, $31\bar{2}$	vw		
.487	302	vw	.485	$21\bar{3}$
.455	$30\bar{4}$	vw	.455	060
.446	204, 122, $20\bar{5}$, 220, $22\bar{1}$, $40\bar{1}$	w		
.433	023, 105, 303, 400, $40\bar{2}$	vw	.433	$23\bar{3}$
.426	015, $12\bar{3}$	vw	.426	$16\bar{1}$
.417	$31\bar{4}$, 401	vw	.417	160
.402	$22\bar{3}$, $30\bar{5}$, $41\bar{2}$	w	.401	201
.3970	115, 313	m		
.3915	$10\bar{6}$, $32\bar{1}$	m	.3903	$16\bar{2}$
.3809	$20\bar{6}$, $32\bar{2}$	vw	.3805	$20\bar{4}$
.3784	304	vw	.3768	$21\bar{4}$
.3740	321, $31\bar{5}$	vw	.3733	033
.3695	$11\bar{6}$, 124, 223, $22\bar{4}$	m	.3689	$26\bar{1}$
.3645	106, $32\bar{3}$	vw	.3657	062
.3361	$13\bar{1}$, $51\bar{1}$	w		
.3347	305, $31\bar{6}$, 413, $51\bar{2}$	vw	.3342	$26\bar{3}$
.3328	007, 206, 131, $41\bar{5}$, $42\bar{2}$	vw	.3326	$33\bar{4}$
.3304	032, 125, 323	vw		
.3233	404, $42\bar{3}$, 421	w	.3239	330
.3214	132, $11\bar{7}$	vw	.3217	$40\bar{3}$
.3199	230, $23\bar{1}$, 315, $40\bar{6}$, 502, 511	vw		
.3126	$12\bar{6}$, $51\bar{4}$	vw	.3122	$36\bar{2}$
.3054	133, 324, 512	vw		
.3037	232	w	.3043	$36\bar{3}$
.3034	$23\bar{3}$	vw	.3033	$43\bar{3}$
.3008	$31\bar{7}$	w	.3009	$36\bar{1}$
.2945	$10\bar{8}$, $20\bar{7}$, $33\bar{2}$, 515	w	.2943	$19\bar{1}$
.2920	$20\bar{8}$, $32\bar{6}$, 423, $52\bar{2}$	m	.2918	$26\bar{4}$
.2908	008, 331, $42\bar{5}$, $60\bar{3}$	s	.2909	034
.2859	$33\bar{3}$, $52\bar{3}$	m	.2859	$33\bar{5}$
.2765	$52\bar{4}$, $51\bar{6}$	vw	.2757	360
.2687	118, 135, $32\bar{7}$, 333, 514	vw		
.2666	406, $50\bar{7}$	vw	.2665	$43\bar{5}$
.2596	317, $13\bar{6}$	m	.2600	400
.2583	009, 040, 326, 416, 523, $51\bar{7}$	m		
.2565	$12\bar{8}$, $60\bar{6}$	w	.2564	203

Another 14 calculated lines, corresponding perfectly to α-TCP spacings, missing from the list above, are undetectable because they are hidden by dominant hydroxyapatite reflections. (s = strong, m = medium, w = weak, vw = very weak).

Of course a complete structural determination, just on the basis of a rather poor powder pattern and accounting for the large low-symmetry cell, cannot be proposed. However, it can be concluded that, despite the marked mimicking of diffraction patterns, $\bar{\alpha}$-TCP has a unit cell clearly distinct from α-TCP and consequently it would be appropriate to call this low-temperature phase γ-TCP.

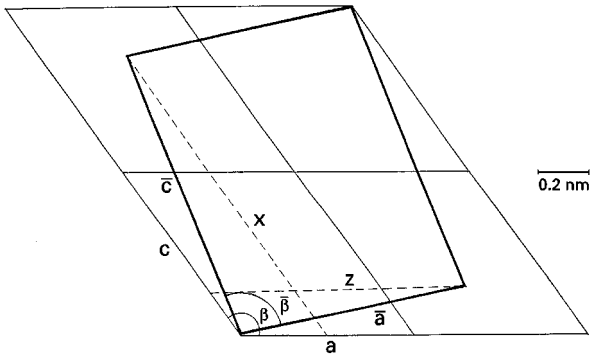

Figure 11 Crystallographic relationships in (0 k 0) projection between low ($\bar{\alpha}$) and high-temperature (α) TCP cells. The dotted traces of $(2\,0\,0)_{\alpha} \equiv (3\,0\,1)_{\bar{\alpha}}(x)$ and $(0\,0\,4)_{\alpha} \equiv (1\,0\,7)_{\bar{\alpha}}(z)$ planes are also shown.

4. Conclusions

Starting from commercial HA powders, isostatically formed and sintered at 1250 °C, materials with high flexural strength were prepared ($\sigma \approx 130$ MPa).

The thermal stability range and typical secondary phase formation in the HA powder were evaluated by TG-DTA and subsequent room temperature XRD analysis; these data were completed by high-temperature XRD investigations, studying also the reversible reactions.

As regards β-TCP bioceramics, their preparation was performed starting from a commercial powder containing a stoichiometric mixture of HA and DCP as precursors. TG-DTA and high-temperature XRD were used to determine the optimal temperature for β-TCP phase formation; the data obtained allowed one to define the stability domains of low-temperature ($\bar{\alpha}$-TCP) and high-temperature α-TCP phases.

Crystallographic analysis was carried out on the less well-known $\bar{\alpha}$-TCP modification, with main diffraction data often confused with those of α-TCP, determining a particular stanfieldite-type monoclinic cell which, although distinct, reproduces the α-TCP powder pattern remarkably well: the definition of this low-temperature phase as γ-TCP seems justified.

Fully dense and translucent β-TCP totally free from α modification was successfully prepared by hot-pressing, attaining a maximum σ value of 120 MPa.

Acknowledgements

The authors wish to thank Jesse-Shirley for kindly supplying the powders used in the present investigation and for high-level contribution. Partial financial support by the BRITE-EURAM project BE-7598-93 is also gratefully acknowledged.

References

1. J. R. VAN WAZER, in "Phosphorus and its compounds", Vols I and II (Interscience, New York, 1958 and 1961).
2. J. S. HANKER and B. L. GIAMMARA, *Science* **242** (1988) 885.
3. H. DENISSEN, C. MANGANO and G. VENINI, in "Hydroxylapatite implants" (Piccin, Padua, 1985).
4. A. ROYER, J. C. VIGUIE, M. HEUGHEBAERT and J. C. HEUGHEBAERT, *J. Mater. Sci. Mater. Med.* **4** (1993) 76.
5. P. E. WANG and T. K. CHAKI, *ibid.* **4** (1993) 150.
6. J. ZHOU, X. ZHANG, J. CHEN, S. ZENG and K. DE GROOT, *ibid.* **4** (1993) 83.
7. H. MONMA and M. GOTO, *Yogyo-Kyokai-Shi* **91** (1983) 473.
8. C. REY, *Biomaterials* **11** (1990) 13.
9. M. JARCHO, C. H. BOLEN, M. B. THOMAS, J. BOBICK, J. F. KAY and R. H. DOREMUS, *J. Mater. Sci.* **11** (1976) 2027.
10. M. TORIYAMA, A. RAVAGLIOLI, A. KRAJEWSKI, G. CELOTTI and A. PIANCASTELLI, *J. Eur. Ceram. Soc.* **16** (1966) 429.
11. E. D. EANES, *Calcif. Tissue Res.* **5** (1970) 133.
12. M. MATHEW, L. W. SCHROEDER, B. DICKENS and W. F. BROWN, *Acta Crystallogr. B* **33** (1977) 1325.
13. T. KANAZAWA, T. UMEGAKI and N. UCHIYAMA, *J. Chem. Technol. Biotechnol.* **32** (1982) 399.
14. T. UMEGAKI, S. SHIBA and T. KANAZAWA, *Yogyo-Kyokai-Shi* **92** (1984) 612.
15. S. INOUE, M. KOBAYASHI and A. ONO, *ibid.* **96** (1988) 182.

Received 8 November 1995
and accepted 29 May 1996